

### Transverse instability of counterpropagating waves in photorefractive media

M. Saffman, D. Montgomery, A. A. Zozulya, K. Kuroda,\* and D. Z. Anderson

Department of Physics and Joint Institute for Laboratory Astrophysics, University of Colorado, Boulder, Colorado 80309-0440

(Received 1 February 1993)

The transverse instability of counterpropagating waves in nonlinear media with a photorefractive or Kerr-type nonlinearity is studied. The problem is formulated for a sluggish nonlinear medium that responds much slower than the optical frequency. In this limit, a general dispersion relation, valid for arbitrary longitudinal variation of the optical intensities, is obtained and solved numerically for several representative cases. It is found that, while photorefractive media provide sufficient nonlinear coupling for the observation of transverse instabilities, such observations may be difficult due to the presence of strong amplified incoherent scattering (fanning) in photorefractive media.

PACS number(s): 42.65.Jx, 42.65.Hw, 42.65.Vh

#### I. INTRODUCTION

Small-scale transverse instability of a single beam [1] or two counterpropagating beams [2] in a Kerr-type nonlinear medium has been known in nonlinear optics for some time. In more recent years a number of theoretical treatments of the subject have appeared [3–7]. A linear analysis shows that the instability manifests itself by the generation of a pair of satellite beams traveling at small angles  $\pm\theta_c$  to the primary beams. The interference of the primary and satellite beams results in a transverse intensity modulation with the characteristic spatial scale  $l_s = 2\pi/\theta_c k_0$ . This transverse modulation is now attracting attention in connection with the formation of patterns in nonlinear optical systems [8]. In the case of counterpropagating beams the nonlinear stage of the instability may, in some cases, result in the formation of hexagonal or square patterns with the size of the patterns being determined by the characteristic spatial scale  $l_s$  of the linear stage. Up to now patterns have been observed in atomic vapors [9] and liquid crystals [10]. It has been suggested [11] that photorefractive crystals may be a suitable choice for nonlinear medium since they exhibit high nonlinearities and the value of nonlinear coupling in the crystal can be easily varied by external means. However, important differences between the Kerr and photorefractive nonlinearities warrant the separate analysis of transverse instabilities of counterpropagating beams that is presented in this paper.

For the case of a single beam propagating through a nonlinear medium the onset of the instability corresponds to the appearance of intensity modulation on its transverse profile with the characteristic modulation period considerably less than the diameter of the beam. As a result of the instability, the beam may break down into several narrower beams (filaments) so it is sometimes referred to (especially in plasma physics) as the filamentation instability. A considerable difference in spatial scales inherent to the problem makes plane-wave analysis a very useful analytical tool in studying the initial stage of the instability. Speaking in this language, a strong plane wave  $F_0$  passing through a Kerr nonlinear medium turns

out to be convectively unstable versus excitation of two spatial sidebands  $F_{\pm 1}$ —two plane waves propagating symmetrically at an angle  $\theta$  to the primary wave [Fig. 1(a)] [1]. The term “convective instability” means that if small seed amplitudes of waves (Fourier harmonics)  $F_{\pm 1}$  are present at the input to the nonlinear medium then they will exponentially grow with distance at the expense of energy supplied by the strong “pumping” wave  $F_0$ . The output amplitudes of waves  $F_{\pm 1}$  are equal to their input amplitudes multiplied by this exponential amplification factor. Instability is possible for a range of angles  $\theta$  between the wave vector  $\mathbf{k}_0$  of the strong plane

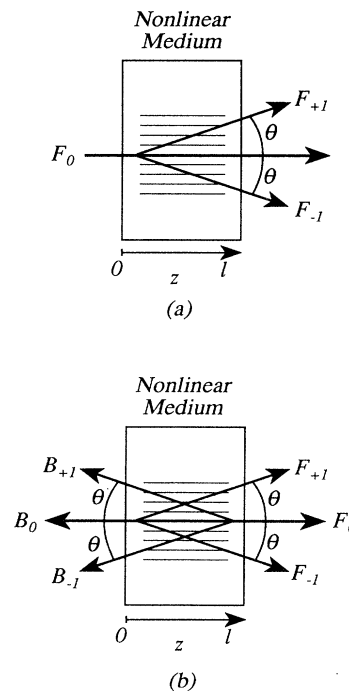


FIG. 1. Geometry of the optical interaction. (a) Excitation of satellite beams by a single primary beam. (b) Excitation of pairs of satellite beams by counterpropagating primary beams.

wave and the wave vectors  $\mathbf{k}_{\pm 1}$  of the sidebands and the characteristic angle (corresponding to the largest amplification) is given by the condition  $\theta_c^2 \propto n_2 |F_0|^2$ , where  $n_2$  is the Kerr coefficient of the medium.

Similarly, two strong plane waves  $F_0$  and  $B_0$  counter-propagating in a Kerr medium turn out to be unstable versus excitation of two pairs of waves:  $F_{\pm 1}$  and  $B_{\pm 1}$  situated as shown in Fig. 1(b) [2]. The characteristic angle  $\theta_c$  between the interacting waves' wave vectors is determined by the expression given earlier. An important difference between this and the previous case is that the system is now absolutely unstable. The term "absolute instability (oscillation)" refers to the situation when in the framework of a system of equations linearized with respect to the amplitudes of weak waves  $F_{\pm 1}$  and  $B_{\pm 1}$  these amplitudes exponentially grow in time provided the intensities of strong pumping waves exceed certain threshold values. Contrary to the case of one pumping beam, the instability starts from any arbitrarily small values of input or initial amplitudes of generated waves and their time growth goes on indefinitely in the framework of the linearized set of equations. Saturation of this growth and steady state can be obtained only if depletion of the pumping beams is taken into account. The final output amplitudes of the generated waves are determined not by their input or initial amplitudes but by how far the intensities of the pumping waves are from their threshold values.

It should be noted that in both cases the transverse instability of beam(s) in Kerr-type media results in the spontaneous appearance of a characteristic spatial scale  $l_s = 2\pi/\theta_c k_0$  in the transverse structure of the beams corresponding to generation of sidebands with either the highest amplification coefficient in the case of a single pump or the lowest threshold of instability in the case of counterpropagating pumps. The general nature of the instability is preserved in photorefractive media, although not the details of the instability threshold conditions, or the structure of patterns that may form in the nonlinear stage of the instability. This is due to several differences between the photorefractive and Kerr-type nonlinearities. In Kerr-type media the nonlinear part of the refractive index  $n_2$  is not (or is only weakly) dependent on the angle  $\theta$  between the interacting waves (see Fig. 1) or, equivalently, on the wave vector  $k_{\perp} = \theta k_0$  of the grating written by the pumping waves with their sidebands ( $F_0$  with  $F_{\pm 1}$  and  $B_0$  with  $B_{\pm 1}$ ) and so the characteristic angle  $\theta_c$  is the result of interplay between the Kerr nonlinearity and diffraction. The nonlinear coupling coefficient (analog of  $n_2$ ) in photorefractive media is strongly dependent on the value of  $k_{\perp}$  and so material properties of the crystal must come into play, imposing their own characteristic spatial scales. Furthermore, the Kerr nonlinearity corresponds to a nonlinear change of phase ( $n_2$  is purely real), whereas the photorefractive nonlinearity is in general complex corresponding to both amplitude and phase changes. The magnitude of the real part of the coupling coefficient can be enhanced by applying an external electric field to the photorefractive crystal, but in general it is impossible to eliminate completely the imaginary part. Also, the dependence of the real and

imaginary parts on the value of  $k_{\perp}$  is different. In addition, photorefractive media are characterized by strong amplified incoherent scattering (fanning) that leads to a dependence of the amplitudes of the primary beams on the axial coordinate, even in the linear stage of the instability.

These effects are studied in Sec. II in the framework of a general dispersion relation, valid for complex coupling coefficients and arbitrary position dependence of the primary beam amplitudes. In Sec. III several particular cases of photorefractive media are discussed, and some conclusions are drawn as to the suitability of photorefractive media for the observation of optical pattern formation.

## II. DISPERSION EQUATION

Consider two strong plane waves  $F_0 \exp(ik_0 z - i\omega_0 t)$  and  $B_0 \exp(-ik_0 z - i\omega_0 t)$  counterpropagating in a nonlinear medium. We will assume that these waves do not interact directly with each other, i.e., the nonlinear medium does not support reflection gratings. This is true in Kerr media when reflection gratings are washed out by, e.g., diffusion. In photorefractive media both transmission and reflection gratings may be significant depending on the geometry of the interacting beams with respect to the crystallographic axes. By assuming that, for example, the beams propagate in a plane whose normal lies along the crystallographic  $c$ -axis reflection gratings may also be neglected in photorefractive media. We further assume that the medium is sluggish and responds only at frequencies much lower than the optical frequency  $\omega_0$  and the characteristic propagation time  $l/c$  ( $l$  is the length of the medium and  $c$  is the speed of light) is small compared to its characteristic relaxation time  $\tau$  (for photorefractive media the latter is of the order of seconds). Let us add a small probe wave  $\delta F_1 \exp[ik_0 z + i\mathbf{k}_{\perp} \cdot \mathbf{r}_{\perp} - i(\omega_0 + \Omega)t]$  ( $|\mathbf{k}_{\perp}| \ll k_0, |\Omega| \ll \omega_0$ ) to this system. Interaction of strong wave  $F_0$  with this probe results in a nonlinear change in the refractive index of the medium proportional to  $F_0 \delta F_1^* \exp(-i\mathbf{k}_{\perp} \cdot \mathbf{r}_{\perp} + i\Omega^* t)$  plus its complex conjugate. The conjugate part supports  $\delta F_1$  whereas scattering of wave  $F_1$  off the first part produces sideband wave  $\delta F_{-1} \exp[ik_0 z - i\mathbf{k}_{\perp} \cdot \mathbf{r}_{\perp} - i(\omega_0 - \Omega^*)t]$ . Similarly scattering of wave  $B_0$  off the grating results in the appearance of waves  $\delta B_{\pm 1}$  [see Fig. 1(b)]. The full set of waves in the linear approximation with respect to the amplitudes of the sidebands is of the form

$$\begin{aligned} F(\mathbf{r}_{\perp}, z, t) &= F_0(z) [1 + F_{+1} \exp(i\mathbf{k}_{\perp} \cdot \mathbf{r}_{\perp} - i\Omega t) \\ &\quad + F_{-1} \exp(-i\mathbf{k}_{\perp} \cdot \mathbf{r}_{\perp} + i\Omega^* t)] \\ &\quad \times \exp(ik_0 z - i\omega_0 t), \\ B(\mathbf{r}_{\perp}, z, t) &= B_0(z) [1 + B_{+1} \exp(i\mathbf{k}_{\perp} \cdot \mathbf{r}_{\perp} - i\Omega t) \\ &\quad + B_{-1} \exp(-i\mathbf{k}_{\perp} \cdot \mathbf{r}_{\perp} + i\Omega^* t)] \\ &\quad \times \exp(-ik_0 z - i\omega_0 t). \end{aligned} \quad (1)$$

Evolution of these waves in photorefractive media is governed by the equations

$$\begin{aligned}
\left[ \frac{\partial}{\partial z} + ik_d \right] F_{+1} &= i\gamma_{nl}[F_{+1} + F_{-1}^* + q(B_{+1} + B_{-1}^*)]/(1+q), \\
\left[ \frac{\partial}{\partial z} - ik_d \right] F_{-1}^* &= -i\gamma_{nl}[F_{+1} + F_{-1}^* + q(B_{+1} + B_{-1}^*)]/(1+q), \\
\left[ \frac{\partial}{\partial z} - ik_d \right] B_{+1} &= -i\gamma_{nl}[F_{+1} + F_{-1}^* + q(B_{+1} + B_{-1}^*)]/(1+q), \\
\left[ \frac{\partial}{\partial z} + ik_d \right] B_{-1}^* &= i\gamma_{nl}[F_{+1} + F_{-1}^* + q(B_{+1} + B_{-1}^*)]/(1+q)
\end{aligned} \tag{2}$$

with the boundary conditions  $F_{+1}(z=0)=F_{-1}(0)=0$ ,  $B_{+1}(z=l)=B_{-1}(l)=0$ , corresponding to an absolute instability. Here  $q(z)=|B_0(z)/F_0(z)|^2$ ,  $k_d=k_1^2/2k_0$ , and  $\gamma_{nl}(\mathbf{k}_l, \Omega)$  is the material and frequency-shift-dependent complex coupling coefficient. Equations (2) also describe sluggish Kerr media with the replacement

$$\gamma_{nl}/(1+q) \rightarrow 2(\omega_0/c)n_2|F_0(z)|^2/(1-i\Omega\tau). \tag{3}$$

Note that in Eqs. (1) and (2) we allow for coordinate dependence of the pumping beams' amplitudes. This will enable us to account for their depletion due to absorption and possible nonlinear processes that are competing with the one under discussion. Of primary concern in photorefractive media is the so-called fanning—a broad-angle incoherent light-induced scattering.

There are several differences between Eqs. (2) and those describing the transverse instability of instantaneous Kerr media [2]. The characteristic relaxation time of the photorefractive medium is much longer than the electromagnetic propagation time through the medium, so the time derivatives in the left-hand sides of Eqs. (2) are neglected. A frequency shift between the pump beams and the excited sidebands enters into Eqs. (2) through the coupling constant  $\gamma_{nl}(\mathbf{k}_l, \Omega)$  that is generally complex. In instantaneous Kerr media the coupling constant is purely real and independent of the frequency shift, which instead enters explicitly into the left-hand sides of Eqs. (2). Because of these differences the solutions of Eqs. (2) will not be comparable with those for instantaneous Kerr media except in the case when the coupling constant is real and the instability in instantaneous Kerr media is static, i.e., there is no frequency shift between the primary waves and the sidebands ( $\Omega=0$ ).

Despite the complex nature of the coupling coefficient Eqs. (2) are simpler than those for instantaneous Kerr media for which no closed analytical expression for the dispersion relation exists except for the case  $\{F_0(z), B_0(z)\} = \text{const}$ . Equations (2) can be solved in closed form for any dependence  $F_0(z), B_0(z)$  and any value of  $\gamma_{nl}(\mathbf{k}_l, \Omega)$  yielding the following dispersion relation for the threshold of the absolute instability:

$$\begin{aligned}
(1-A_1)(1-A_2)-A_3A_4 &= 0, \\
A_1 &= (2\gamma_{nl}k_d/s) \int_0^l dz \frac{q(z)}{1+q(z)} \frac{\sin(k_d z)}{\sin(k_d l)} \sinh[s(z-l)], \\
A_2 &= (2\gamma_{nl}k_d/s) \int_0^l dz \frac{1}{1+q(z)} \frac{\sin[k_d(z-l)]}{\sin(k_d l)} \sinh(sz), \\
A_3 &= (2\gamma_{nl}k_d/s) \int_0^l dz \frac{q(z)}{1+q(z)} \frac{\sin[k_d(z-l)]}{\sin(k_d l)} \\
&\quad \times \sinh[s(z-l)], \\
A_4 &= (2\gamma_{nl}k_d/s) \int_0^l dz \frac{1}{1+q(z)} \frac{\sin(k_d z)}{\sin(k_d l)} \sinh(sz), \\
s &= [k_d(2\gamma_{nl}-k_d)]^{1/2}.
\end{aligned} \tag{4}$$

In the case of  $q(z)=\text{const}$  Eq. (4) reduces to

$$\begin{aligned}
(q+q^{-1}) + [(s/k_d l)^{-1} - (s/k_d)] \sin(k_d l) \sinh(sl) \\
+ 2 \cos(k_d l) \cosh(sl) = 0.
\end{aligned} \tag{5}$$

The case of a sluggish Kerr medium is recovered from Eq. (5) under the replacement (3). Equation (4) or (5) can be solved for  $s$  or  $\gamma_{nl}$  as a function of  $k_d$  not implying any particular dependence  $\gamma_{nl}(k_d)$ . In general, the solutions for  $\gamma_{nl}$  will be complex and there may be a frequency shift between the primary and satellite beams. If attention is restricted to the case of purely real  $\gamma_{nl}$  and no frequency shift, then an equation formally identical to Eq. (5) describes the instability threshold of instantaneous Kerr media, as has been shown in Refs. [4,5].

Equations (4) and (5) have an infinite number of solution branches. In the limiting case of  $k_d \gg |\gamma_{nl}|$ , Eq. (5) gives

$$i\gamma_{nl}l = \pm [-\ln q + i(2N+1)\pi] \tag{6}$$

where  $N$  is an arbitrary integer. Solutions of Eq. (5) for several low-lying branches are presented in Fig. 2. Note that the sign of  $\arg(\gamma_{nl})$  is arbitrary, since if  $\gamma_{nl}$  is a solution of (4), then  $\gamma_{nl}^*$  is also a solution. A direct comparison of the threshold condition for photorefractive media and instantaneous Kerr media may be made when the solutions of Eq. (5) give purely real  $\gamma_{nl}$  and the threshold for instantaneous Kerr media corresponds to zero frequency detuning. Thus the curves in Figs. 2(a) and 2(b) for  $q=1$  are identical to the corresponding curves given in Refs. [3-7]. When comparing the graphs it should be kept in mind that for  $q=1$  Eq. (5) can be written as the product of two terms [6]

$$\begin{aligned}
[\tan(k_d l/2) \tanh(sl/2) - (k_d/s)] \\
\times [\tan(k_d l/2) \tanh(sl/2) + (s/k_d)] = 0
\end{aligned} \tag{7}$$

leading to two solutions for each value of  $k_d l$ . In Fig. 2 we depict only the lowest of the two solutions. For  $q \neq 1$  the curves in Fig. 2 differ from those in Refs. [4,5], which allow for only static instabilities, whereas they appear similar to the results shown in Ref. [7] for instantaneous Kerr media with  $q \neq 1, \Omega \neq 0$ . Note that for  $k_d l$  small,  $\gamma_{nl}$  is purely real irrespective of the value of  $q$ , whereas for large  $k_d l$  only the case  $q=1$  results in real  $\gamma_{nl}$ . The value of  $k_d l$  at which  $\gamma_{nl}$  becomes complex decreases with in-

creasing  $q$  such that the minimum value of  $|\gamma_{nl}|$  is attained with  $\gamma_{nl}$  real when  $q=10$  and with  $\gamma_{nl}$  complex when  $q=100$ .

### III. PHOTOREFRACTIVE MEDIA

Optical beams propagating in photorefractive media interact via the coupling coefficient

$$\gamma_{pr}(\mathbf{k}_\perp, \Omega) = \left[ \frac{\omega_0}{2c} \right] n_{\text{eff}}^3(\mathbf{k}_\perp) r_{\text{eff}}(\mathbf{k}_\perp) E_{\text{SC}}(\mathbf{k}_\perp, \Omega). \quad (8)$$

$$E_{\text{SC}}(\mathbf{k}_\perp, \Omega) = \frac{E_{\text{max}}(\mathbf{k}_\perp)[E_o(\mathbf{k}_\perp) + iE_{\text{diff}}(\mathbf{k}_\perp)]}{[E_{\text{max}}(\mathbf{k}_\perp) + E_{\text{diff}}(\mathbf{k}_\perp) - iE_o(\mathbf{k}_\perp)] - i\Omega t_0[E_\mu(\mathbf{k}_\perp) + E_{\text{diff}}(\mathbf{k}_\perp) - iE_o(\mathbf{k}_\perp)]}, \quad (9)$$

$$E_o(\mathbf{k}_\perp) = E_{\text{app}}(\mathbf{k}_\perp) + E_{\text{pv}}(\mathbf{k}_\perp).$$

The space-charge field is expressed in terms of a number of characteristic fields:  $E_{\text{max}} = eN/\epsilon_{\text{eff}}k_\perp$  ( $e$  is electronic charge,  $N$  is density of traps,  $\epsilon_{\text{eff}} = \hat{\mathbf{k}}_\perp \cdot \epsilon_{\text{static}} \hat{\mathbf{k}}_\perp$ ,  $\epsilon_{\text{static}}$  is the dc dielectric tensor) is the limiting space charge field,  $E_{\text{diff}} = k_B T k_\perp / e$  ( $k_B$  is Boltzmann's constant,  $T$  is absolute

temperature) is the diffusion field,  $E_\mu = \gamma_D N / \mu k_\perp$  ( $\gamma_D$  is the recombination rate of charge carriers,  $\mu$  is the mobility) is the drift field, and  $E_o$ , which is due to the combined effect of the photovoltaic field  $E_{\text{pv}}$  and an externally applied field  $E_{\text{app}} = E_{\text{app},0} \cos(\varphi)$  ( $E_{\text{app},0}$  is the field applied along the  $c$  axis). A simple model is used for the photovoltaic effect such that  $E_{\text{pv}} = E_{\text{pv},0} \cos(\varphi)$ , where  $E_{\text{pv},0}$  (which is assumed to have no dependence on  $\mathbf{k}_\perp$ ) is the local part of the photovoltaic field directed along the  $c$  axis [13]. In the presence of a frequency shift  $\Omega$  between the interacting beams  $E_{\text{SC}}$  is also dependent on the characteristic material response time  $t_0$ , which is inversely proportional to the optical intensity. The values of these parameters may vary considerably between different samples of any particular material. The values given in Table I, which were used for numerical calculations, are meant to be representative; see, e.g., Ref. [14] for references to the original literature.

The phase of  $\gamma_{pr}$  depends on the relative magnitude of the characteristic fields and the frequency shift between the interacting waves. For  $\Omega=0$  and  $E_{\text{diff}} \gg E_{\text{app}}, E_{\text{pv}}$  (large  $\mathbf{k}_\perp$  limit), the charge transport is diffusion dominated and  $\gamma_{pr}$  is mostly imaginary (BaTiO<sub>3</sub> in Table I). When  $E_{\text{max}} \gg E_{\text{app}}, E_{\text{pv}} \gg E_{\text{diff}}$  (small  $\mathbf{k}_\perp$  limit) the charge transport is drift dominated and  $\gamma_{pr}$  is mostly real (LiNbO<sub>3</sub> in Table I). The dependence of  $\gamma_{pr}l$  on  $k_\perp l$  is shown in Fig. 3 for  $\Omega=0$ . In BaTiO<sub>3</sub> the space-charge field has a broad maximum centered at  $k_\perp^*$  where  $E_{\text{diff}}(k_\perp^*) = E_{\text{max}}(k_\perp^*)$ . However, for  $l \sim 1$  cm the corresponding value of  $k_\perp l$  is several thousand, so the maximum is not visible in Fig. 3. For  $k_\perp l \sim \pi$ , corresponding to the minimum instability threshold, the magnitude and phase of  $\gamma_{pr}$  are almost constant in BaTiO<sub>3</sub> in the absence of an applied field. In LiNbO<sub>3</sub> the imaginary part of  $\gamma_{pr}$  varies rapidly for  $k_\perp l \sim \pi$  and an applied field has very little effect due to the strong photovoltaic field.

Comparing Figs. 2 and 3 we may reach the conclusion that a modulational instability should be readily observable in BaTiO<sub>3</sub> with modest applied fields of say 100 V/cm, or in LiNbO<sub>3</sub> with no applied field. However, such a conclusion would be overly optimistic since we have not yet accounted for the space variation of the

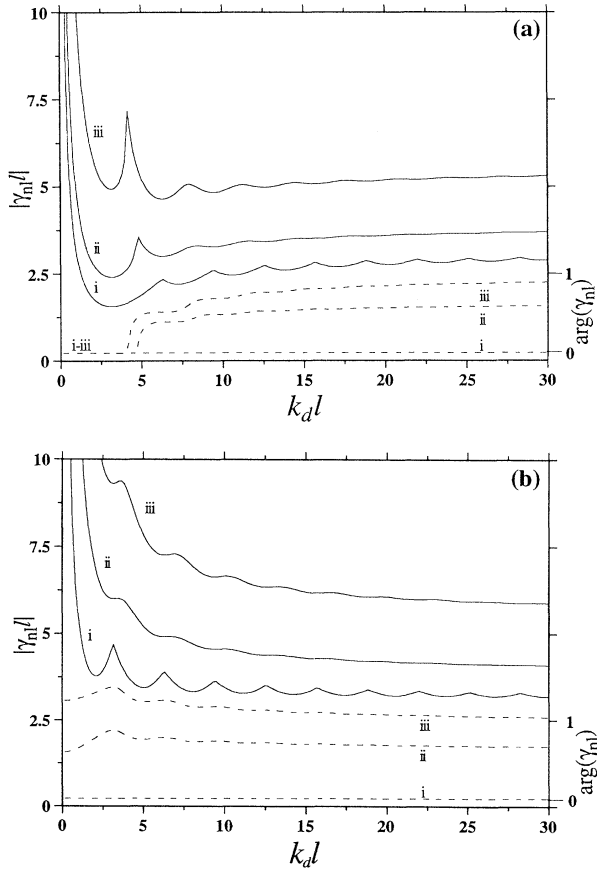


FIG. 2. Dispersion curves for  $q(z)=\text{const}$ : (a) focusing branch with  $\text{Re}(\gamma_{nl}) > 0$  and (b) defocusing branch with  $\text{Re}(\gamma_{nl}) < 0$ . The curves are labeled as  $i$ ,  $q=1$ ;  $ii$ ,  $q=10$ ; and  $iii$ ,  $q=100$ . —,  $|\gamma_{nl}|$ ; - - -,  $\text{arg}(\gamma_{nl})$ .

TABLE I. Physical parameters of some photorefractive crystals.

| Parameter   | BaTiO <sub>3</sub>               | LiNbO <sub>3</sub>    |
|---|----------------------------------|-----------------------|
| Refractive indices                                | $n_o = 2.46$                     | 2.34                  |
|   | $n_e = 2.40$                     | 2.24                  |
| dc dielectric constants ( $\epsilon/\epsilon_0$ ) | $\epsilon_1 = 4300.0$            | 44.0                  |
|   | $\epsilon_3 = 106.0$             | 29.0                  |
|   |                                  |                       |
| Electro-optic coefficients (pm/V)                 | $r_{13} = 19.5$                  | 8.6                   |
|   | $r_{33} = 97.0$                  | 30.8                  |
|   | $r_{42} = 1640.0$                | 28.0                  |
| Photovoltaic field (V/cm)                         | $E_{pv,0} = 10.0$                | $1.0 \times 10^4$     |
| Trap density ( $m^{-3}$ )                         | $N = 4.0 \times 10^{22}$         | $4.0 \times 10^{22}$  |
| Recombination rate ( $m^3/s$ )                    | $\gamma_D = 5.0 \times 10^{-14}$ | $5.0 \times 10^{-14}$ |
| Mobility ( $m^2/V s$ )                            | $\mu = 5.0 \times 10^{-5}$       | $8.0 \times 10^{-5}$  |

beam intensities due to optical losses. The intrinsic absorption in photorefractive media is strongly dependent on the impurity doping level. We measured an intrinsic absorption coefficient of  $\alpha \sim 2 \text{ cm}^{-1}$  in 0.5-cm-thick samples of BaTiO<sub>3</sub> and LiNbO<sub>3</sub> with what appeared to be average dopant levels. These measurements were made using ordinary polarized beams such that  $r_{\text{eff}}$  was small and there was only weak generation of fanning. However, a much stronger loss mechanism exists in the light-induced broad-angle fanning that is characteristic of photorefractive media. Fanning results in very strong de-

pletion of the main beam that can be characterized phenomenologically by an effective absorption coefficient  $\alpha_f$ . Measurements in the same sample of BaTiO<sub>3</sub> using extraordinary polarized beams which induce strong fanning gave a total effective absorption of  $\alpha_T = \alpha + \alpha_f \sim 9 \text{ cm}^{-1}$ , for Gaussian beams of  $\sim 1 \text{ mm}$  diameter. Measurements in the LiNbO<sub>3</sub> sample show that the fanning continuously develops for several hours, leading eventually to virtually total depletion of the central portion of the incident beam. The fanning could be significantly reduced by using narrower beams; however, observation of a transverse instability implies that the beams have a finite width. An interaction length of 1 cm with a beam diameter of 1 mm gives about 20 fringes across the beam at  $k_d l \sim \pi$ .

The quantitative effect of the optical losses on the instability threshold is found by solving Eqs. (4) with  $q(z) = q(0)e^{2\alpha_T z}$ . The dispersion curves for the boundary conditions  $|F_0(0)|^2 = |B_0(l)|^2$ , which were found to minimize the threshold coupling, are shown in Fig. 4. The minimum value of  $|\gamma_{nl}l|$  is now  $\sim 9$  as compared to  $\sim 1.5$  without absorption. In addition, a number of additional branches with comparable  $|\gamma_{nl}l|$  but different phases appear. For the focusing branches [ $\text{Re}(\gamma_{nl}) > 0$ ] and small  $k_d l$  the instability threshold is achieved with purely real  $\gamma_{nl}$ , whereas for large  $k_d l$  the threshold occurs for  $\gamma_{nl}$  complex, except for branch  $i$  which is qualitatively different, being purely real everywhere except for a small region  $36 \leq k_d l \leq 41$  [15]. Apart from this small region this branch is reminiscent of the case  $q = 1$  in Fig. 2, which also has real  $\gamma_{nl}$ . This is somewhat surprising since there are no solutions for  $q = \text{const} \neq 1$  that have real  $\gamma_{nl}$  for all values of  $k_d l$ . This may be related to the choice of  $|F_0(0)|^2 = |B_0(l)|^2$  in Fig. 4, which, despite the fact that  $q = q(z)$ , mimics the  $q = 1$  case as closely as possible. Branches  $ii-vii$  are numbered so that the values of  $k_d l$  at which the solutions for the instability threshold change from purely real to complex increase with increasing branch index. These branches are somewhat reminiscent of those shown in Fig. 2(a) with  $q = \text{const} \neq 1$ . For  $k_d l$  small  $|\gamma_{nl}l|$  is minimized with  $\gamma_{nl}$  real whereas for  $k_d l$  large  $|\gamma_{nl}l|$  is minimized with  $\gamma_{nl}$  complex. At the transitional value of  $k_d l$ , the real and complex solution branches cross resulting in a sharp peak in  $|\gamma_{nl}l|$ . Branches  $ii-ix$  also appear grouped together as in-

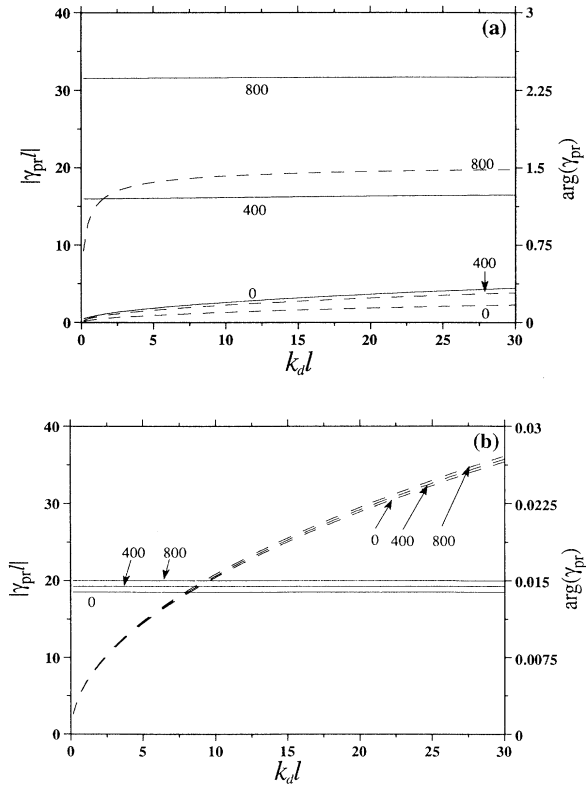


FIG. 3. Photorefractive coupling constant with an applied field: (a) BaTiO<sub>3</sub> ( $\varphi = 22^\circ$ ,  $l = 1 \text{ cm}$ ) and (b) LiNbO<sub>3</sub> ( $\varphi = 0^\circ$ ,  $l = 1 \text{ cm}$ ). The curves are labeled with the value of the applied field in V/cm. —,  $|\gamma_{pr}l|$ ; - - -,  $\arg(\gamma_{pr})$ .

tertained pairs. For  $q(z)=1$  the dispersion relation factors into two terms [Eq. (7)]. Since in that case the two terms both have  $\gamma_{nl}$  real, only the solution that minimizes  $|\gamma_{nl}'|$  is shown in Figs. 2(a) and 2(b). In the more general case of  $q=q(z)$  the dispersion relation is no longer factorable, although the solution branches still appear in intertwined pairs (this behavior is different from that found for  $q=\text{const}\neq 1$ , where the solution branches do not appear in intertwined pairs). In the case of  $q=q(z)$  the intertwined solutions do not have the same value of  $\arg(\gamma_{nl})$  and both solutions are consequently shown in Fig. 4. Additional calculations, not shown in Fig. 4, show that all the branches asymptote to a finite limit for large  $k_d l$ , although a simple analytical expression for the limiting values corresponding to Eq. (6) is no longer available.

All the branches shown in Fig. 4 can be accessed by the photorefractive media since the phase of  $\gamma_{pr}$  depends on  $\Omega$ , which is unconstrained. The dispersion curves of Fig. 4 are normalized by  $\gamma_{pr}$ , as defined by Eq. (8), in Fig. 5. The frequency shift  $\Omega$  has been fixed such that the phase of  $\gamma_{pr}$  is equal to the phase of  $\gamma_{nl}$  and at each value of  $k_d l$  the branch which minimizes  $|\gamma_{nl}/\gamma_{pr}|$  is chosen. Values of the ordinate less than 1 in Fig. 5 imply that the thresh-

old condition has been exceeded, and instabilities may be observable.

Even accounting for optical losses it appears theoretically possible to observe transverse instabilities of counterpropagating beams in photorefractive media. The instability should be accessible with applied fields of several hundred V/cm in BaTiO<sub>3</sub> and without applied fields in LiNbO<sub>3</sub>. Additional calculations, not reported here, indicate that the threshold should be several times lower still for the same applied field if SBN:75 (Sr<sub>0.75</sub>Ba<sub>0.25</sub>Nb<sub>2</sub>O<sub>6</sub>) is substituted for BaTiO<sub>3</sub>. The reason for the lower threshold in this case is that  $\epsilon_3$  ( $\epsilon_3$  is the 33 component of  $\epsilon_{\text{static}}$ ) is about 30 times larger in SBN:75 than in BaTiO<sub>3</sub> which reduces  $E_{\text{max}}$  by a factor of 30 and greatly increases the grating phase shift for the same applied field. It should be mentioned that while a modulational instability in one transverse dimension corresponding to the appearance of fringes appears possible, it is unlikely that patterns with hexagonal or other two-dimensional symmetries may be observed in photorefractives. In order to have symmetric interactions in the transverse plane it is necessary to propagate along the symmetry axis of the crystal which leads to very weak coupling, far below the threshold for transverse instabilities.

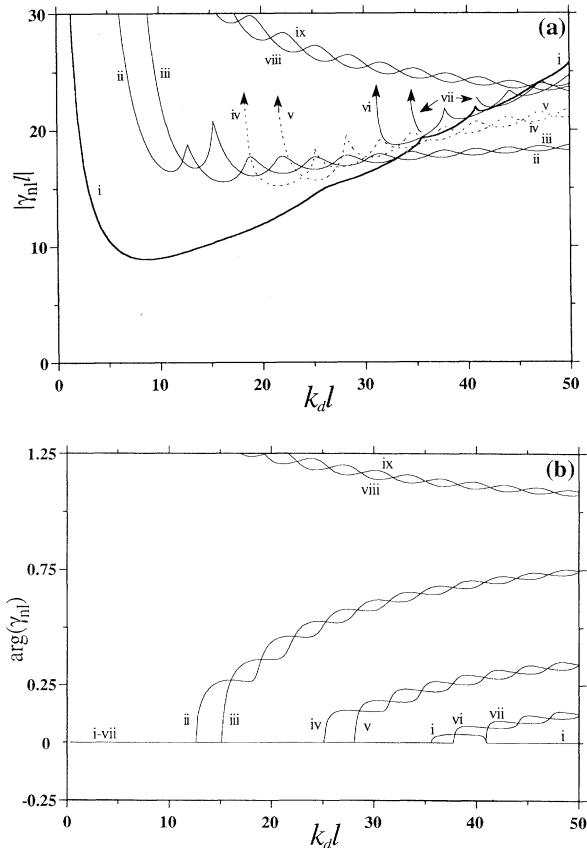


FIG. 4. Dispersion curves in the presence of optical losses for  $\alpha_T l=9$ : (a)  $|\gamma_{nl}|$  and (b)  $\arg(\gamma_{nl})$ . Curves *i-vii* correspond to focusing branches with  $\text{Re}(\gamma_{nl})>0$  while curves *viii* and *ix* correspond to defocusing branches with  $\text{Re}(\gamma_{nl})<0$ .

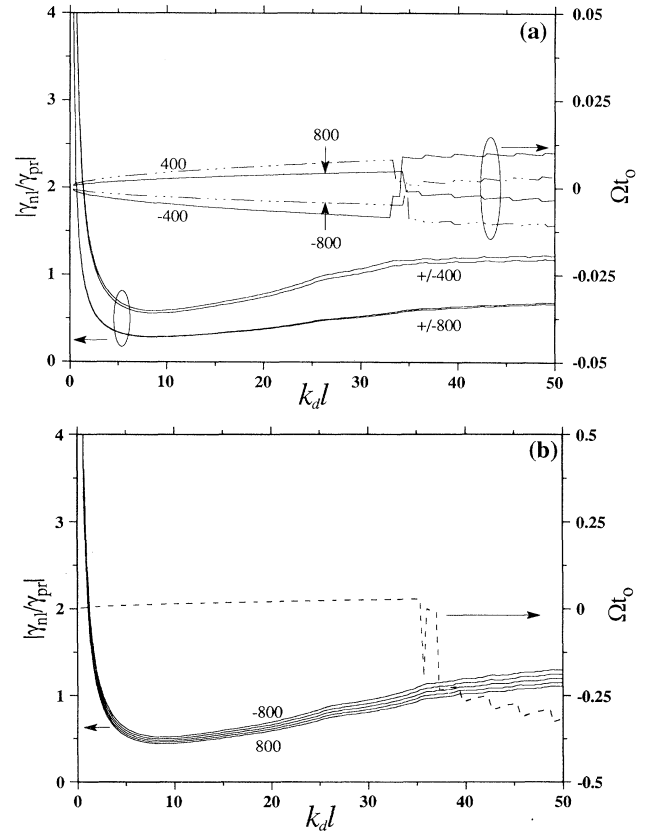


FIG. 5. Normalized dispersion curves: (a) BaTiO<sub>3</sub> and (b) LiNbO<sub>3</sub>. The curves are labeled with the value of the applied field in V/cm. The zero applied field curve is not shown for BaTiO<sub>3</sub> since it is more than ten times below threshold. The abrupt jumps in  $\Omega t_0$  are due to the minimum threshold solution jumping between the different branches shown in Fig. 4.

We remain pessimistic as to the likelihood of any such observations in the transmission geometry studied here. The photorefractive coupling coefficients are in principle large enough for the observation of instabilities. Unfortunately, strong photorefractive coupling is intimately connected with strong fanning. The calculations reported here account for fanning losses in the simplest possible way, as an effective additional absorption. But the effect of fanning may be even more deleterious. The fanning light fills a broad angular region that may mask the otherwise observable instability. In addition, when the fanning is strong, as is the case under conditions favorable for the observation of instabilities, the incident beam acquires a distorted transverse profile and is no longer well described by a plane-wave model. The instability threshold may indeed be many times higher when the beams are strongly distorted.

After completion of this work we became aware of the recent observation of hexagonal patterns due to the formation of reflection gratings in a photorefractive medium [16]. Geometries in which reflection gratings are dominant significantly improve the situation since they allow

narrow beams to be employed which greatly reduces the level of fanning. We expect that general features of our results will still be applicable to the reflection geometry, although quantitative predictions of instability thresholds would have to be recalculated. The most significant difference being that the direct coupling between the counterpropagating primary beams leads to a different variation of the beam intensity ratio  $q(z)$  from that considered here.

#### ACKNOWLEDGMENTS

This work was supported by NSF group grant in Atomic, Molecular and Optical Physics No. Phy 90-12244, U.S. Air Force Office of Scientific Research Grant No. AFOSR-90-0198, Office of Naval Research Grant No. N00014-88-K-0083, and the Optoelectronic Computing Systems Center, a NSF Engineering Research Center. K.K. would like to acknowledge support provided by the Ministry of Education, Japan. M. Saffman thanks the U.S. Air Force Office of Scientific Research for support.

---

\*Permanent address: Institute of Industrial Science, University of Tokyo, Roppongi, Minato-ku, Tokyo 106, Japan.

- [1] V. I. Bespalov and V. I. Talanov, Pis'ma, Zh. Eksp. Teor. Fiz. **3**, 471 (1966) [JETP Lett. **3**, 307 (1966)].
- [2] S. N. Vlasov and V. I. Talanov, in *Optical Phase Conjugation in Nonlinear Media*, edited by V. I. Bespalov (Institute of Applied Physics, USSR Academy of Sciences, Gorki, 1979), p. 85; S. N. Vlasov and E. V. Sheinina, Izv. Vyssh. Uchebn. Zaved. Radiofiz. **26**, 20 (1983) [Radiophys. Quant. Electron. **27**, 15 (1983)].
- [3] W. J. Firth and C. Paré, Opt. Lett. **13**, 1096 (1988).
- [4] G. Grynberg and J. Paye, Europhys. Lett. **8**, 29 (1989).
- [5] G. G. Luther and C. J. McKinstrie, J. Opt. Soc. Am. B **7**, 1125 (1990).
- [6] W. J. Firth, A. Fitzgerald, and C. Paré, J. Opt. Soc. Am. B **7**, 1087 (1990).
- [7] G. G. Luther and C. J. McKinstrie, J. Opt. Soc. Am. B **9**, 1047 (1992).
- [8] L. A. Lugiato, Phys. Rep. **219**, 293 (1992); C. O. Weiss, *ibid.* **219**, 311 (1992).
- [9] G. Grynberg, E. Le Bihan, P. Verkerk, P. Simoneau, J. R. R. Leite, D. Bloch, S. Le Boiteux, and M. Ducloy, Opt. Commun. **67**, 363 (1988); A. Petrossian, M. Pinard, A. Maître, J.-Y. Courtois, and G. Grynberg, Europhys. Lett. **18**, 689 (1992).
- [10] R. Macdonald and H. J. Eichler, Opt. Commun. **89**, 289 (1992).
- [11] G. D'Alessandro and W. J. Firth, Phys. Rev. Lett. **66**, 2597 (1991).
- [12] N. V. Kukhtarev, V. B. Markov, S. G. Odulov, M. S. Soskin, and V. L. Vinetskii, Ferroelectrics **22**, 949 (1979).
- [13] B. Sturman, Kvant. Elektr. **7**, 483 (1980) [Sov. J. Quantum Electron. **10**, 276 (1980)].
- [14] *Photorefractive Materials and Their Applications I*, edited by P. Günter and J. P. Huignard (Springer-Verlag, Berlin, 1988); M. P. Petrov, S. I. Stepanov, and A. V. Khomenko, *Photorefractive Crystals in Coherent Optical Systems* (Springer-Verlag, Berlin, 1991).
- [15] For  $36 \leq k_d l \leq 41$  branch *i*, which is everywhere else purely real, becomes complex, and branch *vii* disappears completely. This unusual behavior may be related to the fact that the branches lie in close proximity in this region. If the behavior shown by the other branches were followed here, then both branch *i* and branch *vii* would be purely real and have very similar magnitudes for  $36 \leq k_d l \leq 41$ .
- [16] T. Honda, Opt. Lett. **18**, 598 (1993).